Applied Energy 231 (2018) 167–178

Contents lists available at ScienceDirect

Applied Energy

journal homepage: www.elsevier.com/locate/apenergy

Application of density functional theory in studying CO_2 capture with TiO_2-supported K_2CO_3 being an example

Qiaoyun Qin[a,1], Hongyan Liu[a,b,1], Riguang Zhang[a,c], Lixia Ling[a], Maohong Fan[c,*], Baojun Wang[a,*]

[a] Key Laboratory of Coal Science and Technology of Ministry of Education and Shanxi Province, Taiyuan University of Technology, Taiyuan, Shanxi 030024, China
[b] College of Chemistry and Environmental Engineering, Shanxi Datong University, Datong, Shanxi 037009, China
[c] Departments of Chemical and Petroleum Engineering, University of Wyoming, Laramie, WY 82071, USA

HIGHLIGHTS

- Preadsorbed H_2O makes CO_2 adsorption increase over K_2CO_3/TiO_2 sorbent.
- CO_2 and H_2O prefer to adsorb at the interface of K_2CO_3/TiO_2.
- Carbonation reaction is governed by H_2O dissociation.
- The better K-based sorbent for CO_2 capture is proposed.

GRAPHICAL ABSTRACT

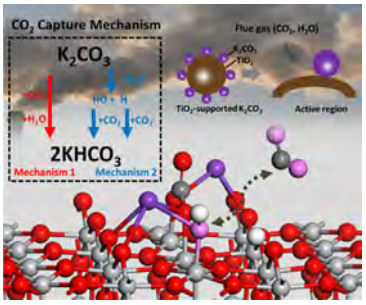

ARTICLE INFO

Keywords:
Density-functional theory
CO_2 capture
K_2CO_3
Rutile

ABSTRACT

Solid sorbents based CO_2 capture has become increasingly important. Great progress has been achieved with experimental studies in this area. However, the density functional theory based capture study on the function of H_2O in CO_2 capture is lacking. This research was designed to make progress in this important area with TiO_2-supported K_2CO_3 being an example. Due to its high cost-effectiveness, dry K_2CO_3 is a promising sorbent for capturing CO_2. Yet challenges remain in accelerating the rate of the absorption process. The study of mechanism of the effect of H_2O on CO_2 adsorption as well as the carbonation reaction can help select and design better support for the sorbent. Up to now, it is open. In this work, the adsorption and reaction of CO_2 over K_2CO_3 loaded on a rutile (1 1 0) surface have been studied using theoretical calculations. The results show that the CO_2 adsorption is increased when H_2O appears, and carbonation reaction mainly occurs at the interfaces of K_2CO_3/TiO_2 includes bicarbonate formation resulting from the reactions of CO_2 with OH via H_2O dissociation and CO_3 anion with transferred H via H_2O dissociation combining. In addition, H transfer step appears when support TiO_2 exists compared to that on pure K_2CO_3 sorbent. The kinetic modeling indicates that the H_2O dissociation may limit the carbonation reaction. Therefore, H_2O-dissociative or high OH coverage TiO_2 support material can assist CO_2 sorption with the solid K_2CO_3 based CO_2 capture technology. It is expected that the theoretical study sheds light on the preparation of cost-effective CO_2 sorbents in the future.

* Corresponding authors.
E-mail addresses: mfan@uwyo.edu (M. Fan), wangbaojun@tyut.edu.cn (B. Wang).
[1] The two authors have equal contribution to the paper.

https://doi.org/10.1016/j.apenergy.2018.09.114
Received 24 May 2018; Received in revised form 1 August 2018; Accepted 9 September 2018

1. Introduction

Global warming caused by greenhouse gas emission has, in recent years, been recognized as a major risk to mankind [1–3]. Carbon dioxide (CO_2) is one of the major greenhouse gases, and it has been reported that one-third of CO_2 emissions worldwide come from fossil fuel-based power plants [4]. Hence, capturing CO_2 emitted from the flue gas of power plants has been considered to be a potentially effective approach to controlling atmospheric CO_2 levels.

Methods explored to remove CO_2 from flue gas include membrane separation (separated CO_2 from a CO_2–N_2 mixed gas) [5], absorption with a solvent (CO_2 absorption with aqueous, blends of monoethanolamine and N-methyldiethanolamine, etc.) [6,7], and adsorption on molecular sieves (adsorption–desorption on molecular sieves by pressure or temperature swing) [8,9]. However, these methods are costly and consume large amounts of energy. One of the improved techniques for the removal of CO_2 is the chemical absorption of CO_2 with dry renewable K_2CO_3 sorbents [10,11] and K_2CO_3-promoted hydrotalcite sorbents [12,13]. Hydrotalcites have the unique property of CO_2 sorption at high temperatures (200–600 °C), which can be applied to the direct CO_2 removal from flue gases without cooling process. The equilibrium CO_2 sorption uptake of hydrotalcite could be much more increased by impregnation with K_2CO_3. However, the regeneration temperature is high. Meanwhile, K_2CO_3 sorbents are employed in CO_2 absorption from flue gas of fossil-fueled based thermal power plants at low temperatures (50–90 °C). The use of K_2CO_3 sorbents can be highly cost effective and an energy efficient way to remove CO_2 from flue gas following the reaction $K_2CO_3 + CO_2 + H_2O \leftrightarrow 2KHCO_3$. In addition, the global carbonation reaction rate for pure K_2CO_3 is rather slow [14]. We therefore suggested that, in preparation support, a promoter or special technique may be needed to modify the structure of the K_2CO_3 surfaces to strengthen the adsorption of CO_2, thereby further improving conversion of carbonate to the bicarbonate based our theoretical calculation.

Some supports such as SiO_2, Al_2O_3, CaO, MgO, TiO_2 and activated carbon (AC) have been used in alkali metal-based sorbents to enhance CO_2 capture. Lee et al. [15–18] and Zhao et al. [19–22] found that sorbents of K_2CO_3/AC, K_2CO_3/TiO_2, K_2CO_3/MgO, and K_2CO_3/Al_2O_3 showed excellent CO_2 capture capacity; on the other hand, those sorbents were completely regenerated above 130, 130, 350, and 400 °C, respectively. However, the CO_2 capture capacities of K_2CO_3/Al_2O_3 and K_2CO_3/MgO decreased during multiple absorption/regeneration cycles (absorption at 60 °C and regeneration at 150 °C), mainly due to the formation of $KAl(CO_3)_2(OH)_2$, $K_2Mg(CO_3)_2$, and $K_2Mg(CO_3)_2{\cdot}4(H_2O)$, which did not completely convert to the original K_2CO_3 phase. However, unlike K_2CO_3/Al_2O_3 and K_2CO_3/MgO, a $KHCO_3$ crystal structure was formed during CO_2 absorption on K_2CO_3/AC and K_2CO_3/TiO_2 sorbent. This phase could easily be converted into the original phase during regeneration, even at a low temperature (130 °C). Meanwhile, Lee et al. [23] investigated the structure effects of potassium-based TiO_2 (anatase) sorbents on CO_2 capture capacity. Under the temperature of calcine, the CO_2 capture capacity of the sorbent was reduced due to the undesired formations of $K_2Ti_2O_5$, $K_2Ti_6O_{13}$, and $K_2Ti_4O_9$. However, the rutile structure of TiO_2 can prevent the formation of new structures such as $K_2Ti_2O_5$ and $K_2Ti_6O_{13}$, thus significantly affect CO_2 capture capacity. In addition, $TiO(OH)_2$ has been found to be a promising catalytic support for not only improving CO_2 capture of solid sorbents [24,25], but dramatically reducing energy consumption [26].

The reaction mechanism for CO_2 uptake by K_2CO_3 and the role of H_2O in the reaction are open. Mahinpey et al. [27] reported that K_2CO_3 hydration to form $K_2CO_3{\cdot}1.5H_2O$ and carbonation occur in parallel, without direct conversion from $K_2CO_3{\cdot}1.5H_2O$ to $KHCO_3$. Further, Mahinpey et al. [28] discussed the kinetic behavior of solid K_2CO_3 under CO_2 capture and brought up that the carbonation reaction are limited by adsorption, not chemical reaction based on proposed Langmuir-Hinshelwood model. However, Zhao et al. [29] and Li et al. [30] suggested that $K_2CO_3{\cdot}1.5H_2O$ can react with CO_2 in a fast kinetic rate. Meanwhile, Li et al. [31] determined that hydration reaction occurred through the reaction between K_2CO_3 and the steam, and approximately 75% of K_2CO_3 were converted to $K_2CO_3{\cdot}1.5H_2O$ in high temperature, however, $KHCO_3$ cannot directly react with the steam to produce $K_2CO_3{\cdot}1.5H_2O$. Although there have been some experimental explorations into the mechanism of carbonation reaction, it is difficult to understand the mechanism completely due to the complexity of CO_2 capture with K_2CO_3 sorbent. Quantum mechanics calculation is a useful tool to help clarify the detail of the reaction. Gao et al. [32] investigated the carbonation reaction only on pure K_2CO_3 with monoclinic structure using the density functional theory (DFT) method, proposing that the carbonation reaction occurs via the single “one-step mechanism”, i.e., the OH group resulting from the dissociation of H_2O attacking the C of CO_2 to form bicarbonate. Also, the same reaction on low index surfaces of pure K_2CO_3 with both cubic and monoclinic structures was studied, and it was confirmed that the carbonation reaction can directly proceed either via the interaction between OH resulting from H_2O dissociation and the C atom of CO_2 on monoclinic and hexagonal K_2CO_3, or between the OH group from H_2O dissociation reacting and gaseous CO_2 on hexagonal K_2CO_3, i.e., the carbonation reaction is both a “one-step” and a “two-step mechanism” [14]. Further, investigating the CO_2 desorption reaction on an anatase-TiO_2 (1 0 1) surface by DFT method, Wu et al. [33] concluded that the formation of the unstable intermediary $TiO(OH)^+$ and OH^- by the adsorption of H_2O on the catalyst TiO_2 surface can accelerate the reaction. However, in their work the initial states are not $KHCO_3$, but rather hydroxyl and carbonyl states. On the other hand, adsorption and carbonation of CO_2 and H_2O on pure rutile or anatase have been investigated extensively. For instance, investigating the co-adsorption properties of CO_2 and H_2O on rutile of TiO_2 (1 1 0) using a dispersion-corrected DFT study, Sorescu et al. [34] found that the co-adsorbed H_2O or OH species slightly increase the CO_2 adsorption energies. Other influence factors, including the solvent effect [35] and the effect of excess electron and hole [36], have also been investigated. However, CO_2 captured by TiO_2-supported K_2CO_3 sorbent still has not been investigated using a theoretical method. Does TiO_2-supported K_2CO_3 capture CO_2 better than pure K_2CO_3 or clean TiO_2? What is the capture mechanism in detail? Where is the active site? The above questions are open.

In order to increase CO_2 capture efficiency, it is imperative to make clear the mechanism by which K_2CO_3/TiO_2 captures CO_2. This work focuses mainly on the mechanisms of the K_2CO_3/TiO_2 (rutile) capture of CO_2 through DFT calculation, due to the relatively simpler capture/regeneration mechanism on rutile-supported K_2CO_3 than other media. At the same time, the results are compared with those using pure K_2CO_3 or clean TiO_2 so that the CO_2 capture mechanism can be comprehended better.

2. Computational details

2.1. Computational methods

The DFT approach has been proved to be very successful in modeling the ground state properties of various structures, and has thus been widely used to predict the structural and energetic properties. DFT with Hubbard U correction is to treat the strong on-site Coulomb repulsion, which is not correctly described by LDA or GGA, mainly employed to calculate and analysis the refined electronic structures. At present, geometric optimization and transition state search cannot yet be carried out using the DFT + U method in the CASTEP code, largely because DFT alone has been considered fairly reliable in most cases for structural optimization, resulting in lattice parameters below 1% level of inaccuracy [37,38].

Previous experimental and theoretical studies have demonstrated that CO_2 molecules interact relatively weakly with the rutile(1 1 0) and K_2CO_3 surface. Thus, one might presume that long-range dispersion

interactions would be important for characterizing the CO_2-surface interactions.

In this study, DFT calculations were performed to measure CO_2 and H_2O adsorption and carbonate formation processes on the surface of K_2CO_3 loading on TiO_2 using periodic slab models [39–42]. All calculations were performed using the Cambridge Sequential Total Energy Package (CASTEP) [38] of Materials Studio 8.0 from Accelrys with the General Gradient Approximation (GGA) Perdew-Wang 1991 (PW91) functional [43]; the pseudo potential is ultrasoft. The DFT-D3 correction [44] was incorporated with the PW91 functional to handle dispersion interaction, and a large convergence of the plane wave expansion was obtained with an energy cutoff of 340 eV. For geometry optimization, the Brillouin zone was sampled in a $2 \times 2 \times 1$ Monkhorst-Pack set [45]. The geometries were not optimized until the energy, force and max displacement converged to 2.0×10^{-5} eV/atom, 0.05 eV/Å and 2×10^{-3} Å, respectively. Useful thermodynamic data can be calculated based on calculation of the phonon frequencies.

Before adspecies adsorption, the binding energy of K_2CO_3 and TiO_2, was evaluated according to the following formula:

$$E_b = E_{(K_2CO_3/TiO_2)} - E_{(K_2CO_3)} - E_{(TiO_2)} \quad (1)$$

where $E_{(K_2CO_3/TiO_2)}$ is the total energy of the whole system when K_2CO_3 is deposited on TiO_2, $E_{(K_2CO_3)}$ is calculated by putting a K_2CO_3 unit in a 10 Å × 10 Å × 10 Å box, and $E_{(TiO_2)}$ is the energy of clean TiO_2 (1 1 0) slab.

The adsorption energy is evaluated according to the following formula:

$$E_{ads} = E_{(adsorbate/K_2CO_3/TiO_2)} - E_{(K_2CO_3/TiO_2)} - E_{(adsorbate)} \quad (2)$$

where $E_{(adsorbate/K_2CO_3/TiO_2)}$ is the total energy of the surface of K_2CO_3/TiO_2 with adsorbate; $E_{(adsorbate)}$ is the energy of the free adsorbate (H_2O or CO_2), which is calculated by putting adsorbate in a 10 Å × 10 Å × 10 Å box; And $E_{(K_2CO_3/TiO_2)}$ is the total energy of K_2CO_3 supported on TiO_2.

The adsorption energy of CO_2 co-adsorption with other species is defined as:

$$E_{co-ads} = E_{(CO_2/H_2O/K_2CO_3/TiO_2)} - E_{(H_2O/K_2CO_3/TiO_2)} - E_{(CO_2)} \quad (3)$$

where $E_{(CO_2/H_2O/K_2CO_3/TiO_2)}$ is the total energy of the surface of K_2CO_3/TiO_2 with adsorbates H_2O and CO_2, $E_{(H_2O/K_2CO_3/TiO_2)}$ is the total energy of the surface of K_2CO_3/TiO_2 only with adsorbate H_2O, and $E_{(CO_2)}$ is the energy of the free CO_2 obtained by putting CO_2 in a 10 Å × 10 Å × 10 Å box.

The standard molar Gibbs free energy for gaseous species and adsorbed species can be calculated using the following formula [46]:

$$G^{\theta}(T, p) = E_{total} + E_{ZPE} + U^{\theta} - TS^{\theta} + \gamma RT\left[1 + \ln\left(\frac{p}{p^{\theta}}\right)\right] \quad (4)$$

$$U^{\theta}_{Vib} = RT \sum_i \frac{h\nu_i/k_B T}{e^{h\nu_i/k_B T} - 1} \quad (5)$$

$$S^{\theta} = R \sum_{i=1}^{n} -\ln(1 - e^{h\nu_i/k_B T}) + \frac{h\nu_i/k_B T}{e^{h\nu_i/k_B T} - 1} \quad (6)$$

where E_{total} refers to the total energy obtained directly from DFT calculations, R is the gas constant, p is the partial pressure of the gas-phase molecules, and γ is 0 for surface adsorbed species, and 1 for gaseous molecule; E_{ZPE} is the zero-point vibrational energy; U^{θ} and S^{θ} are the thermal energy and entropy, respectively.

In addition, the activation energy E_a and reaction energy ΔE are calculated according to the following formula:

$$E_a = E_{TS} - E_R \quad (7)$$

$$\Delta E = E_P - E_R \quad (8)$$

where E_R, E_{TS} and E_P are the energies of reactants, transition states and products in an elementary reaction, respectively.

The reaction rate constants (k) can be obtained using harmonic transition state theory [47]:

$$k = \frac{k_B T}{h} \frac{q_{TS}}{q_R} \exp\left(-\frac{E_{act}}{k_B T}\right) \quad (9)$$

$$q = \frac{1}{\prod_{i=1}^{Vibration} 1 - \exp\left(-\frac{h\nu_i}{k_B T}\right)} \quad (10)$$

where k_B is the Boltzmann constant, T is the actual temperature (350 K), and E_{act} represents the DFT-calculated and zero-point-corrected activation energy.

2.2. Computational model

Unlike a sorbent prepared using anatase structure TiO_2, Lee et al. [23] determined that sorbent prepared by impregnating TiO_2 having a rutile structure with 30% K_2CO_3 is of the constant capacity of CO_2 capture. Additionally, it is easy to regenerate K_2CO_3 supported by TiO_2 with rutile structure after CO_2 capture. Therefore, rutile is considered as the support in this work.

The crystallographic data for rutile bulk structure used in this work was taken from the Inorganic Crystal Structure Database (ICSD-200391). The structure was subsequently geometrically optimized (energy minimization) to test the methods used in this work, and the calculated lattice parameters of bulk rutile are a = 4.646 Å and c/a = 0.637 Å, which are in good agreement with the experimental results of a = 4.594 Å and c/a = 0.644 [48] (i.e., the deviations are only 1.13% and 1.08%, respectively). This indicates that the employed method is suitable for carrying out the calculations in this work.

Being of the minimal energy, (1 1 0) surface of rutile is preferentially expressed in macroscopic crystal morphologies, and has been assumed to dominate the surface chemistry [49]. Herein, a (4 × 2) supercell was used to represent rutile TiO_2(1 1 0) containing five layers, with the bottom two layers kept frozen at bulk optimized positions and the upper three layers allowed to relax. Vacuum thickness (size of unit cell perpendicular to slab-slab thickness) was set to be 15 Å, which is large enough to avoid unnecessary potential surface-surface interaction. The electrons transfers were also calculated for comparison through Mulliken population analysis.

For the computational model, a K_2CO_3 monomer supported on the rutile (1 1 0) surface was used to represent the active component of K_2CO_3 deposited on TiO_2, in which the structure of K_2CO_3 is composed of nearly planar CO_3 anions and K cations coordinated to oxygen atoms.

3. Results and discussion

3.1. TiO_2 supported K_2CO_3

There are three types of surface structures for carbonate anion deposited on oxide, i.e., bidendate, mondendate and bridge structures [50]; the position of the K species on the TiO_2 (1 1 0) is between the bridging oxygen [51]. Based on the above position and surface structures, the possible configurations of K_2CO_3 deposited on TiO_2(1 1 0) were explored, and the results showed that carbonate anion of K_2CO_3 favors binding on the surface of TiO_2 in bridge structure, i.e., the two O atoms from carbonate bind with two Ti atoms of surface. The distances are 1.967 and 1.969 Å, respectively, and the distances of K cations and O atoms of the surface are 2.589 and 2.800 Å, respectively (Fig. 1). The calculated binding energy is -711.1 kJ·mol^{-1}, indicating that K_2CO_3 is bound substantially stronger on TiO_2 (1 1 0).

We also performed PDOS analysis for the supported configurations (Fig. 2). There are many resonance peaks between s-, p-from O in K_2CO_3 and s-, p-, d-from Ti, confirming strong interaction between K_2CO_3 and TiO_2 support, which indicating that the new phase is not easy to form in the calcination process. This is consistent with the experimental results

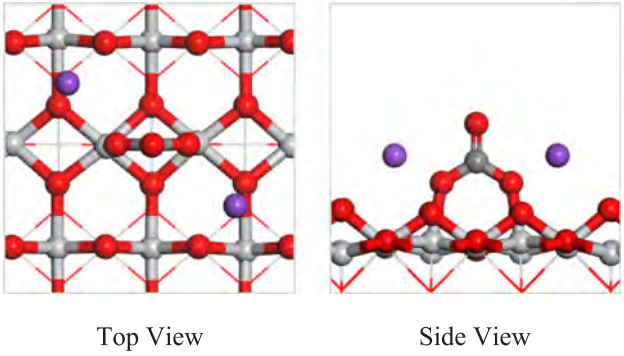

Fig. 1. The main model of K_2CO_3 loaded on (4 × 2) rutile of TiO_2 (1 0 0) surface.

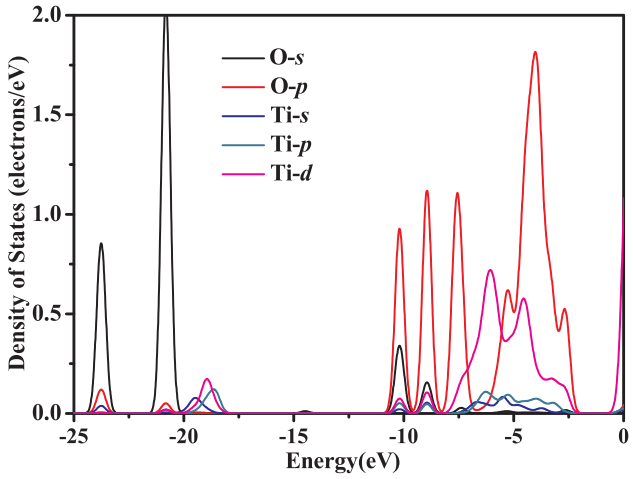

Fig. 2. PDOS plots for K_2CO_3 deposit on TiO_2 (1 1 0) surface. (O from K_2CO_3 and Ti from TiO_2).

[23] that sorbent prepared by impreganation of TiO_2 having the rutile structure almost did not transform into new structure such as $K_2Ti_2O_5$ and $K_2Ti_6O_{13}$ below 500 °C.

3.2. CO_2 and H_2O adsorption

For the K_2CO_3 loaded on (4 × 2) rutile (1 1 0) surface, investigation of the adsorption of CO_2 and H_2O on the surface is lacking. Here, stable adsorption configurations were found, marked as C(1)–C(4) for CO_2 adsorption, W(1)–W(2) for H_2O molecular adsorption, and DW(1)–DW (2) for H_2O dissociative adsorption (Fig. 3). The corresponding adsorption energies and structural parameters, as well as Mulliken charges, are listed in Table 1.

3.2.1. CO_2 adsorption

For CO_2 adsorption, there are four different binding configurations of CO_2 on K_2CO_3 loaded on TiO_2 (1 1 0) surface. In C(1) and C(2), the CO_2 molecule is adsorbed at the interface of K_2CO_3 and TiO_2, in which an O atom from adsorbed CO_2 is located above a Ti site, and the whole CO_2 maintains a linear configuration, tilting relative to the surface normally toward a nearby bridge O site on the TiO_2 surface. The distances of Ti and the O of CO_2 are 2.755 and 2.809 Å, and the distances of K and the nearest neighboring O of CO_2 are 2.873 and 3.003 Å, respectively. The adsorption energies are −43.4 and −40.5 kJ·mol^{-1}, respectively. In C(3) and C(4), the CO_2 molecule is adsorbed on the support TiO_2. CO_2 is adsorbed along the Ti row in a lying-down configuration in C(3) with the adsorption energy of −31.8 kJ·mol^{-1}. Meanwhile, CO_2 is adsorbed on the top of the bridge oxygen atom rather than in the middle of two bridge oxygen atoms in C(4), with the adsorption energy of −23.2 kJ·mol^{-1}. Analyzed by the Mulliken charge, it is found that there are a few electrons transferred from the interface of K_2CO_3/TiO_2 as well as the surface of TiO_2 to the CO_2, which changes the C—O bond slightly.

The adsorbed configurations discussed above are similar to those of CO_2 adsorbed on TiO_2 (1 1 0) with or without the H_2O environment obtained by Liu et al. [35]. However, the adsorption energies are larger than those on pure TiO_2 (1 1 0), but smaller than those on TiO_2(1 1 0) with H_2O solvent effect and pure K_2CO_3 [14]. In order to compare the effect of the K_2CO_3/TiO_2 interface on the adsorption of CO_2, we also investigated the adsorption of CO_2 on clean TiO_2 (1 1 0). After removing the K_2CO_3 from TiO_2, there are three configurations for the adsorption of CO_2 on TiO_2 (1 1 0) corresponding to C(1), C(3) and C(4) in Fig. 3 (note: C(1) is equal to C(2) in such a case). The calculated adsorption energies are −33.8, −32.8 and −23.2 kJ·mol^{-1} on clean TiO_2 (1 1 0) surface, respectively. The results are almost consistent with our adsorption energies obtained with CO_2 adsorbed on the support TiO_2 of K_2CO_3/TiO_2, but lower than that with CO_2 adsorbed at the interface of K_2CO_3/TiO_2. Therefore, we will use the results from the support TiO_2 of K_2CO_3/TiO_2 instead of those from pure TiO_2 in the following study. In addition, our calculated results about CO_2 adsorbed on rutile (1 1 0) surface with DFT-D3 are almost in agreement with those by Sorescu et al. [34], whose results are −42.5, 37.6 and −21.2 kJ·mol^{-1} using DFT + U method. This can further confirm that DFT-D3 method also is suitable for carrying out the calculation to investigate the geometry and reaction process in this work.

On the other hand, the heat of adsorption, which is a measure of the energy required for regeneration, should be substantially low. Heats of adsorption are generally in the range of −25 to −50 kJ·mol^{-1} for physisorption cases [52]. Interestingly, our calculated adsorption energies of CO_2 are −23.2 to −43.4 kJ·mol^{-1}, which is consistent with the experimental results. The identical results guarantee the confidence of our calculated data.

3.2.2. H_2O adsorption

3.2.2.1. Molecular adsorption. There are two different binding configurations of H_2O over K_2CO_3 loaded on TiO_2 (1 1 0) surface. In the most stable adsorption configuration, W(2), the O atom of the H_2O molecule interacts with a surface Ti atom and a K cation, and forms a hydrogen bond to a surface O_b atom; the adsorption energy of this configuration is −98.4 kJ·mol^{-1}. However, in the other adsorption configuration, W(1), the O atom of the H_2O molecule interacts only with a surface Ti atom and forms a hydrogen bond to a surface O_b atom; the adsorption energy of this configuration is -81.0 kJ·mol^{-1}, which is smaller than that in W(2) due to less interaction with the K_2CO_3. Obviously, H_2O prefers to adsorb at the interface between K_2CO_3 and TiO_2 in W(2) than on the surface of support TiO_2 in W(1). It has been found that the adsorption energy of H_2O over K_2CO_3 deposited on TiO_2 (1 1 0) surface is a little stronger than that on TiO_2 (1 1 0) by Bandura et al. [53], who obtained the adsorption energy of −92.0 kJ·mol^{-1}. Those are stronger than the result obtained by Sahoo et al. [54], which showed the binding strength of H_2O of 60.8 kJ·mol^{-1}. In addition, the adsorption of H_2O on pure K_2CO_3 up to 126.4 kJ·mol^{-1} [14] is stronger than that at the interface of K_2CO_3/TiO_2 and support of TiO_2.

3.2.2.2. Dissociative adsorption. In recent studies, it was found that H_2O molecules not only remain intact when adsorbed at low temperature at monolayer coverage, but also that a small portion of H_2O monomers can dissociate, with the fraction of such dissociated monomers increasing with increased temperature [55,56]. Accordingly, we also investigated the dissociative adsorption of H_2O on K_2CO_3/TiO_2. Starting from the stable adsorption of H_2O on the sorbent with the configurations of W(1) and W(2), the dissociated H_2O molecule leads to formation of a terminal hydroxyl (marked as OH_t, adsorbed on the top of Ti) and a bridging hydroxyl (marked as OH_b, in which O is from TiO_2, which expresses that H_b is adsorbed on O). The distances between the H

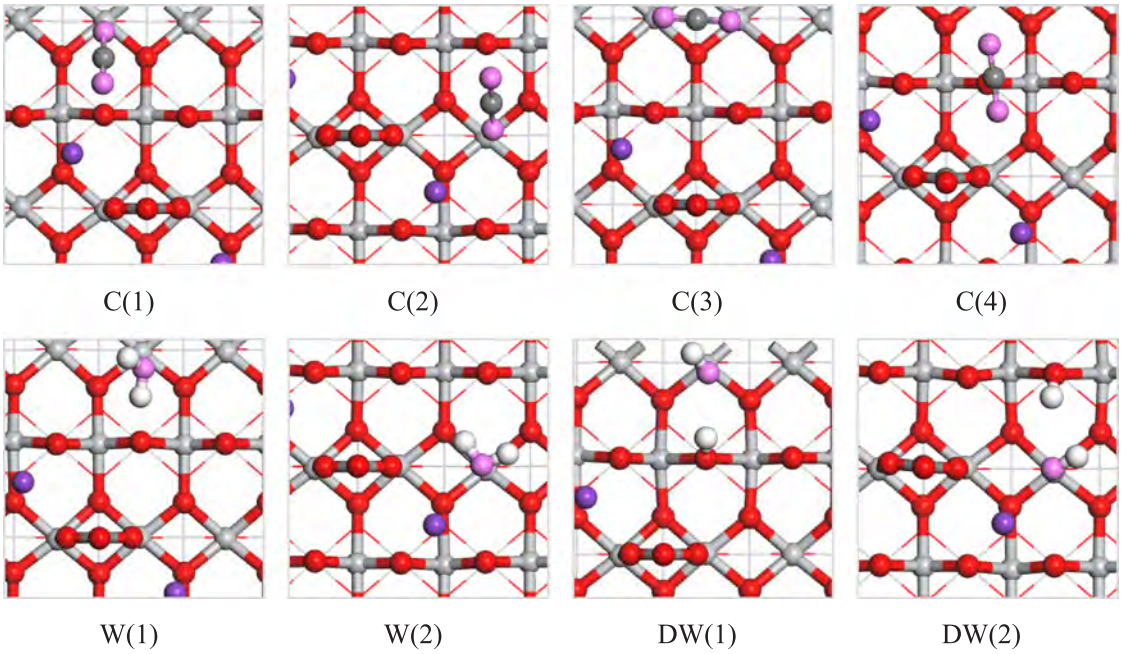

Fig. 3. Top views of the main adsorption configurations of CO_2 and H_2O on the K_2CO_3-loaded TiO_2 (1 1 0) surface [configurations C(1)–C(4) for CO_2 adsorption; configurations W(1) and W(2) for H_2O molecular adsorption; configurations DW(1) and DW(2) for H_2O dissociative adsorption]. For increased clarity, the oxygen atoms of CO_2 and H_2O are indicated in pink, and the oxygen atoms of the slab are indicated in red. (For interpretation of the references to color in this figure legend, the reader is referred to the web version of this article.)

in OH_b and the O atom in OH_t are 2.431 and 2.259 Å in DW(1) and DW (2), and the adsorption energies of H_2O are −70.4 and −117.7 kJ·mol^{-1}, respectively.

Whether H_2O is adsorbed in the form of molecule or dissociation, the interaction between H_2O and the K_2CO_3 loaded on TiO_2 (1 1 0) surface is much stronger than that between CO_2 and the K_2CO_3 loaded on TiO_2 (1 1 0) surface. This implies that when H_2O is adsorbed firstly on the TiO_2 (1 1 0) surface, CO_2 molecules will not be able to displace the adsorbed H_2O molecules. This finding suggests that pre-adsorbed H_2O blocks CO_2 adsorption, and it is consistent with the results on pure TiO_2(1 1 0) obtained by Henderson et al. [57] and Sorescu et al. [34].

3.3. CO_2-H_2O co-adsorption

Because the adsorption of H_2O is far stronger than that of CO_2, when CO_2 is being captured, pre-adsorbed H_2O has an effect on CO_2 adsorption that cannot be ignored in the process. Therefore, the co-adsorption of CO_2-H_2O needs to be investigated.

3.3.1. CO_2 and molecular H_2O co-adsorption

We considered co-adsorption of H_2O with a CO_2 molecule on K_2CO_3/TiO_2, based on the aforementioned four-adsorption configuration of CO_2. The largely CO_2-H_2O configurations are marked as M(1)–M (4), shown in Fig. 4, and the corresponding adsorption energies, structural parameters, and Mulliken charges are given in Table 2.

For all co-adsorption configurations, M(1), M(3) and M(4) represent CO_2 adsorbed on a Ti site based on the W(2) structure of H_2O adsorption on a TiO_2 surface; meanwhile, M(2) expresses CO_2 adsorbed on a Ti site based on the W(1) structure of H_2O adsorption at the interface of K_2CO_3/TiO_2. These adsorbed configurations cause the formation of a hydrogen bond between the H_2O molecule and one of the O atoms of CO_2, with the bond angle of the CO_2 molecule being slightly decreased, which leads to a slight increase in CO_2 adsorption energy. The adsorption energies of M(1), M(2), M(3) and M(4) are increased by 1.9,

Table 1
Adsorption energies, representative geometrical parameters, and *Mulliken charge* of CO_2 and H_2O molecules adsorbed at different sites on K_2CO_3 loaded on TiO_2 (1 1 0) surface.

Configurations	r(Ti-O_c)[a] (Å)	r(C-O_b)[b] (Å)	r(K-O_c)[a] (Å)	r(C-O) (Å)	α(OCO) (°)	E_{ads} (kJ·mol^{-1})	Charge (*e*)
CO_2(gas)				1.184, 1.184	180.0		
C1	2.755	2.927	2.873	1.176, 1.183	177.2	−43.4	−0.03
C2	2.809	2.958	3.003	1.176, 1.186	176.4	−40.5	−0.07
C3	2.763, 2.999	–	4.986	1.181, 1.182	178.6	−31.8	−0.05
C4	–	2.655	4.405	1.180, 1.185	176.2	−23.2	−0.06
Configurations	r(Ti-O_w)[c] (Å)	r(O_b-H)[c] (Å)	r(K-O_w)[c] (Å)	r(O_w-H)[c] (Å)	α(HO_wH) (°)	E_{ads} (kJ·mol^{-1})	Charge (*e*)
H_2O(gas)				0.979, 0.979	104.2		
W1	2.355	1.916	–	0.975, 0.999	109.2	−81.0	0.03
W2	2.538	2.735	2.711	0.980, 0.988	104.2	−98.4	0.02
DW(1)	1.842	0.981	–	0.978, 2.257	–	−70.4	0.04
DW(2)	1.903	0.981	2.632	0.977, 2.431	–	−117.7	−0.06

[a] The O_c is refer to O atom of CO_2 molecule.
[b] The O_b is refer to a generic surface bridging O atom.
[c] The O_w is refer to O atom of H_2O molecule.

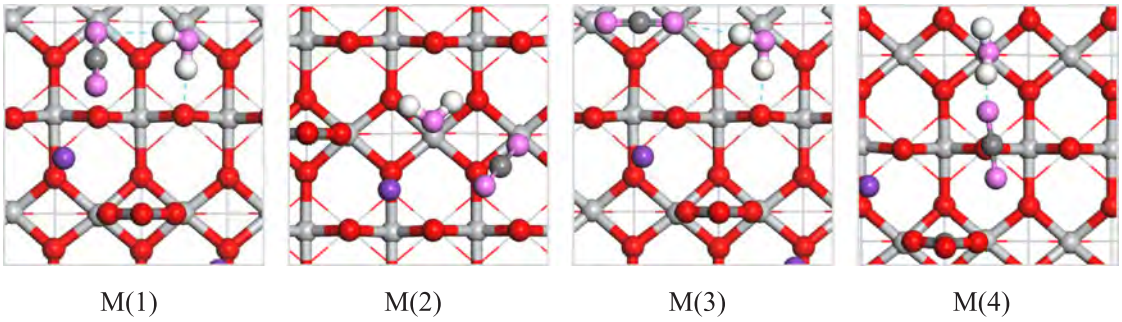

Fig. 4. Top views of the main co-adsorption configurations of CO_2 and H_2O species over the K_2CO_3 loaded on rutile (1 1 0) surfaces. For increased clarity, the oxygen atoms of CO_2 and H_2O are indicated in pink, and the oxygen atoms of the slab are indicated in red. (For interpretation of the references to color in this figure legend, the reader is referred to the web version of this article.)

17.4, 8.7 and 18.3 kJ·mol^{-1}, respectively. Certainly, the smallest increase from C(1) to M(1) it is for these co-adsorption configurations, while the biggest increment it is from C(4) to M(4). Sorescu et al. [34] concluded that the largest enhancement of the CO_2 adsorption energy may be observed for configurations that are most weakly bound to the surface in the absence of H_2O, which is consistent with our findings. In addition, the presence of the H_2O molecule may increase the adsorption stability of the CO_2 molecule. Even if the co-adsorption of H_2O with CO_2 makes the adsorption of CO_2 increase in the above four cases, the most stable co-adsorption configuration of CO_2 with H_2O is CO_2 adsorption at the interface of K_2CO_3/TiO_2 with M(2) configuration. In addition, the adsorption energy increments of CO_2 is larger on K_2CO_3/TiO_2 (1 1 0) than those on pure TiO_2 (1 1 0) [34]. Liu et al. [35] also found that the co-adsorbed H_2O can increase the binding energy of CO_2 by 6.1 to 11.6 kJ·mol^{-1} in both the vacuum and solvent cases.

3.3.2. CO_2 and dissociative H_2O co-adsorption

Because adsorbed H_2O molecules can dissociate to form OH_t and OH_b species, we need to consider the interaction of CO_2 with the two types of hydroxyl groups when studying the co-adsorption of CO_2 and H_2O molecules on a K_2CO_3-loaded TiO_2 (1 1 0) surface. Starting from relatively stable adsorption configurations of CO_2, we have also analyzed the co-adsorption of a CO_2 molecule over K_2CO_3 loaded on a (4 × 2) TiO_2 (1 1 0) surface with terminal OH_t and bridging OH_b species, as well as with H. The corresponding co-adsorption configurations, denoted DA(1)–DA(4), are shown in Fig. 5; the corresponding adsorption energies (E_{ads}) and structural parameters as well as Mulliken charges, are given in Table 3.

Similar to the case with CO_2 and H_2O co-adsorption, the co-adsorption of both OH and H also enhances the adsorption energy of CO_2 by formation of a hydrogen bond between the OH species and one of the O atoms of CO_2. For the stable adsorption configurations of CO_2 with structures of C(1), C(2) and C(3), corresponding to the co-adsorption configurations DA(1)–DA(3) in Fig. 5, the CO_2 adsorption energies are increased by 4.8, 2.9 and 8.7 kJ·mol^{-1}, respectively. Nevertheless, the adsorption energies increment of C(2) to DA(2) is smaller than that of co-adsorption with H_2O of C(2) to MA(2). For the most stable co-adsorption configuration of DA(1), this result is almost consistent with the calculation by Yin et al. [35], who found that largest binding energy is 50.7 kJ·mol^{-1} without solvation effect. For the adsorption configurations of CO_2 in C(4), the adsorption energy has the largest increment by 19.3 kJ·mol^{-1}. Although the adsorption energies of CO_2 in C(1)–C(4) structures increase in varying degrees when dissociative H_2O co-exists, the most stable structure of CO_2 adsorption is still CO_2 adsorption in C(1) mode, accompanied by H_2O dissociative adsorption with DW(2).

In summary, the main effect of co-adsorption of H_2O in molecular and dissociative states on the adsorption of CO_2 on a K_2CO_3/TiO_2 sorbent is a slight increase in the stability of the CO_2 adsorption on the sorbent. Our results are consistent with Mahinpey et al. [28], who explained that the increase in adsorption energy of CO_2 is due mainly to the fact that the activated $K_2CO_3{\cdot}[H_2O]_{ads}$ basic site might have a much greater affinity for interacting with the acidic CO_2 than neutral K_2CO_3.

Among the various co-adsorption configurations, the co-adsorption of molecular H_2O or dissociative H_2O and CO_2 makes the weakest CO_2 adsorption enhance in maximum extent compared to the CO_2 adsorption alone; however, the strongest adsorption of CO_2 is still the one in C(1) whether the co-adsorption of CO_2 with molecular H_2O and dissociative H_2O or CO_2 adsorption alone.

3.4. Bicarbonate formation pathway

In our previous work, the formation of bicarbonate may have been facilitated through the “one-step mechanism” and the “two-step mechanism” [14]. Herein, we also investigated bicarbonate formation reaction through the two mechanisms.

3.4.1. Bicarbonate formation from “one-step mechanism”

Beginning with the most stable co-adsorption configurations for H_2O and CO_2 in M(2), bicarbonate formation requires a path in which the OH dissociates from the H_2O molecule and attacks the adsorbed CO_2; the other H in H_2O molecule transfers to the CO_3 anion. The optimized geometries of the reactant, transition state (TS) and product are shown in Fig. 6, the corresponding transition state structural parameters, reaction activation energy and reaction energy are listed in Table 4. In the transition state (TS), the H-O bond length in the adsorbed H_2O is elongated from 0.984 to 2.481 Å, and the distance

Table 2
Adsorption energies, representative geometrical parameters and the total *Mulliken* charge of a CO_2 molecule co-adsorbed with a H_2O molecule on K_2CO_3 loaded on TiO_2 (1 1 0) surface.

Configurations	r(Ti-O_c)[a] (Å)	r(C-O_b)[b] (Å)	r(K-O_c)[a] (Å)	r(H···O) (Å)	r(C-O) (Å)	α(OCO) (°)	ΔE_{ads} (kJ·mol^{-1})	Charge (*e*)
M1	2.799	2.912	2.911	2.331	1.179, 1.182	177.0	−45.3	−0.04
M2	2.096	2.991	3.417	2.743	1.176, 1.181	176.0	−57.9	−0.05
M3	2.797, 3.027	–	–	2.371	1.180, 1.183	178.5	−40.5	−0.05
M4	–	2.608	4.323	1.733	1.173, 1.190	174.3	−41.5	−0.01

[a] The O_c is refer to O atom of CO_2 molecule.
[b] The O_b is refer to a generic surface bridging O atom.

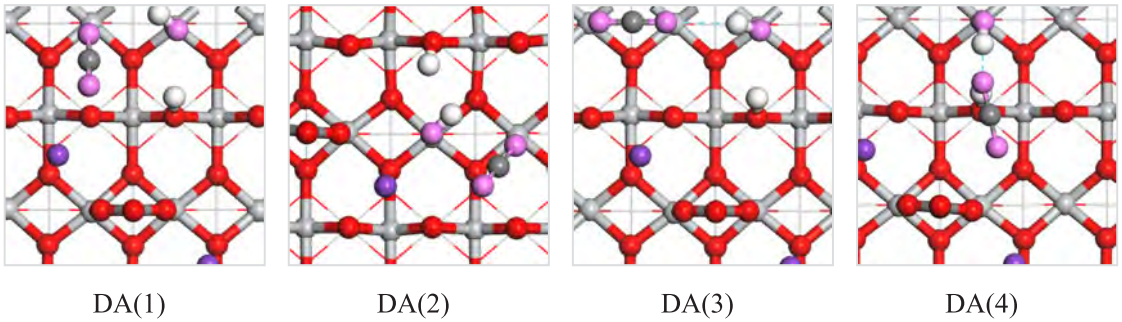

Fig. 5. Top views of the main co-adsorption configurations of CO_2 with a dissociative H_2O molecule over the K_2CO_3 loaded on TiO_2 (1 1 0) surfaces. For increased clarity, the oxygen atoms of CO_2 and H_2O are indicated in pink, and the oxygen atoms of the slab are indicated in red. (For interpretation of the references to color in this figure legend, the reader is referred to the web version of this article.)

between the C atom of CO_2 and O atom of H_2O is shortened from 2.910 to 2.108 Å. The calculated values of the activation energy and reaction energy are 146.6 and 66.6 kJ·mol^{-1}, respectively. The activation energy is far greater than those on low-index surfaces of monoclinic and hexagonal K_2CO_3 obtained in our previous work [14], which are 19.3 to 70.4 kJ·mol^{-1}.

3.4.2. Bicarbonate formation from "two-step mechanism"

In our previous work, the "two-step mechanism" involved H_2O dissociating into OH and H, then OH attacking CO_2 to form a HCO_3 anion, and H combining with CO_3 to form HCO_3 [14]. On the TiO_2-supported K_2CO_3 sorbent, there are two areas we will take into account in this study, namely, the surface of TiO_2 (1 1 0) and the interface of K_2CO_3/TiO_2 (1 1 0). Different from pure K_2CO_3, the H from H_2O dissociation must migrate on the sorbent of K_2CO_3/TiO_2 and then combine with a CO_3 anion to form a HCO_3 anion, rather than combining directly with CO_3 in the sorbent to form HCO_3. Therefore, the "two-step mechanism" includes an additional process of H migration besides the aforementioned two steps, as opposed to that on a pure K_2CO_3 sorbent.

3.4.2.1. H_2O dissociation. Starting from the stable adsorption of H_2O on the surface with structures of W(1) and W(2), we have analyzed the dissociation of the H_2O molecule. The dissociated H_2O molecule leads to the formation of a terminal hydroxyl (OH_t) and a bridging hydroxyl (OH_b), as shown in DW(1) and DW(2) in Fig. 3, and the structures of the transition state are shown in Fig. 7, the corresponding transition state structural parameters, reaction activation energy and reaction energy are listed in Table 5. The resulting activation energy and reaction energy obtained from calculations using a transition searching method are 48.2 and 8.7 kJ·mol^{-1} from W(1) to DW(1), and 37.6 and −13.5 kJ·mol^{-1} from W(2) to DW(2). The results show that H_2O dissociation at the interface of K_2CO_3/TiO_2 has a relatively low reaction barrier and that the reaction process is exothermic, indicating that it is easy to dissociate H_2O at the interface of K_2CO_3/TiO_2. Although H_2O dissociation on the surface of TiO_2 also has low activation energy, the reaction is endothermic. The entire process from adsorption of H_2O to dissociation into OH and H is exothermic and of a low heat entropy change. We therefore believe that H_2O is also easy to dissociate on the surface of TiO_2.

From the above results, one can conclude that the adsorption of H_2O in molecular states is easy to dissociate, whether H_2O adsorbed at the interface of K_2CO_3/TiO_2 or on the surface of TiO_2. Further, because of the lower activation energy at the interface of K_2CO_3/TiO_2 compared to that on the surface of TiO_2, one can conclude that the presence of K_2CO_3 on TiO_2 promotes the dissociation of H_2O, which is similar to the conclusion obtained by Grinter et al. [51] that a more favorable H_2O dissociation is fostered by the presence of K atoms on the surface. On the other hand, the activation energy of H_2O dissociation at the interface of K_2CO_3/TiO_2 sorbent is lower than that on pure K_2CO_3 (55.0 kJ·mol^{-1}) [14], indicating that the support TiO_2 not only facilitates K_2CO_3 dispersion, but also makes H_2O dissociation easier.

3.4.2.2. H proton transfer. Based on the dissociative configurations of DA(1) and DA(2), the calculated result shows that the reaction of the H proton cannot combine directly with CO_3 anions, as that on a pure K_2CO_3 sorbent. Therefore, H transfer is dispensable for the mechanism. The direct H transfer from OH_b to the O atoms of CO_3 anions is unfavorable due to the greater distance of H proton transfer. Taking into account the presence of H_2O molecules in this situation, we think that H_2O molecules can also participate in this process, as shown in Fig. 8, the corresponding transition state structural parameters, reaction activation energy and reaction energy are listed in Table 6.

The resulting activation energies and reaction energies are 54.0 and 19.3 kJ·mol^{-1} for DA(1) to P1 via TS2-2-1, and 59.8 and −8.7 kJ·mol^{-1}for DA(2) to P2 via TS2-2-2, respectively. The calculated results confirmed that the presence of the H_2O molecule makes the H transfer possible.

3.4.2.3. OH_t reaction with CO_2. We explored the bicarbonate formation reaction mechanism by reacting CO_2 and OH_t based on the co-adsorption configuration of CO_2 and OH in DA(1) and DA(2) structures. The calculated reaction pathways of the CO_2 and OH are shown in Fig. 9, the corresponding transition state structural parameters, reaction activation energy and reaction energy are listed in Table 7, wherein the reaction refers to the OH_t attacking nearby CO_2 molecules adsorbed at the Ti site. The resulting activation energies are

Table 3
Adsorption energies, representative geometrical parameters and variation of the total *Mulliken charge* of a CO_2 molecule co-adsorbed with a dissociative H_2O molecule on K_2CO_3 loaded on TiO_2 (1 1 0) surface.

Configurations	r(Ti-O_c)[a] (Å)	r(O_b-C)[b] (Å)	r(K-O_c)[a] (Å)	r(H···O_c)[a] (Å)	r(C-O) (Å)	α(OCO) (°)	ΔE_{ads} (kJ·mol^{-1})	Charge (*e*)
DA1	2.839	2.934	2.888	2.576	1.177, 1.183	177.0	−48.2	−0.04
DA2	2.690	3.021	3.506	2.497	1.175, 1.184	177.7	−43.4	−0.07
DA3	3.070, 2.784	–	–	2.508	1.180, 1.182	178.6	−40.5	−0.05
DA4	–	2.671	4.245	1.763	1.175, 1.187	175.0	−42.5	−0.03

[a] The O_c is refer to O atom of CO_2 molecule.
[b] The O_b is refer to a generic surface bridging O atom.

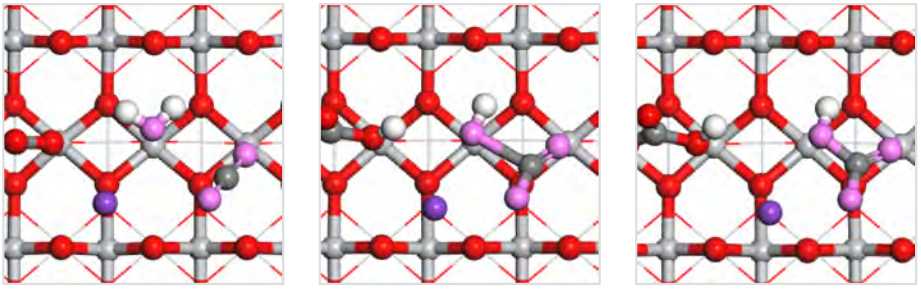

Fig. 6. The pathways for reaction of co-adsorption configurations of CO_2 and H_2O species M(2). For increased clarity, the oxygen atoms of OH_t and H_2O are indicated in pink, and the oxygen atoms of the slab are indicated in red. (For interpretation of the references to color in this figure legend, the reader is referred to the web version of this article.)

44.4 and 57.9 kJ·mol^{-1}, respectively. Meanwhile, the processes are slightly exothermic, with reaction energies of −7.7 and −28.9 kJ·mol^{-1}. Obviously, the reaction barrier is slightly lower on the surface of TiO_2 than on the interface of K_2CO_3/TiO_2. Our calculated activation energy on the surface of TiO_2 is almost equal to that (48.2 kJ·mol^{-1}) on clean TiO_2 [35], and higher than that (25.1 kJ·mol^{-1}) on pure K_2CO_3 [14].

The activation energies in the above elementary reactions are similar, which leads to difficulty in judging the carbonate performance. Therefore, the microkinetic modeling for the CO_2 capture on K_2CO_3/TiO_2 will be investigated, and the rate of bicarbonate formation is then calculated at each site.

3.5. Microkinetic modeling

For the "one-step mechanism", only reactions at the interface of K_2CO_3/TiO_2 were taken into account. The corresponding activation free energies G_a, reaction free energies ΔG and rate constant k are summarized in Table 8 (R1, R2 and R6).

Reactions (1) and (2) (R1 and R2) are presumed to represent equilibrium, with equilibrium coverages of CO_2 and H_2O determined as a function of partial pressures, and assuming competitive Langmuir adsorption and excluding possible other adsorbed species, such as bicarbonate.

These were calculated by the following formula:

$$\theta_{H_2O} = \frac{K_{H_2O}P_{H_2O}}{1 + K_{H_2O}P_{H_2O} + K_{CO_2}P_{CO_2}} \quad (11)$$

$$\theta_{CO_2} = \frac{K_{CO_2}P_{CO_2}}{1 + K_{H_2O}P_{H_2O} + K_{CO_2}P_{CO_2}} \quad (12)$$

The equilibrium constants for CO_2 and H_2O adsorption were estimated by the formula [47]:

$$K = \exp[-(E_{ads} - T\Delta S)/k_B T] \quad (13)$$

where ΔS is the entropy change of gas-phase CO_2 or H_2O, which are obtained from NIST Chemistry Web Book. The reaction rate r for bicarbonate formation (R6) at each site was calculated by the following formula:

$$r_6 = k_6 \theta_{H_2O} \theta_{CO_2} \quad (14)$$

The Gibbs adsorption free energy, equilibrium constant of CO_2 and H_2O are listed in Table 9, with all reaction conditions at 350 K; a gas mixture of 0.15 atm CO_2, 0.15 atm H_2O, and 70% N_2, and a total pressure of 1 atm were considered [15].

The Gibbs free energy of CO_2 adsorption is less than that of H_2O, so the CO_2 adsorption equilibrium constant is exceedingly smaller than that of H_2O. The calculated reaction rate constant k, θ_{CO_2}, θ_{H_2O}, and reaction rate are 2.06×10^{-10} s^{-1}, 8.25×10^{-8}, 0.9999 and 1.70×10^{-17} s^{-1}, respectively. The reaction rate for bicarbonate formation from M(2) is small due to the smaller reaction rate constant k and coverage of CO_2, θ_{CO_2}. This is similar to bicarbonate formation on a K_2CO_3 (0 0 1) surface obtained by Gao et al. [32], who found that the reaction rate for bicarbonate formation is small because the CO_2 adsorbed fraction is very small. We also calculated the reaction rates on the low index on pure K_2CO_3 based on our previous investigation, listed in Table 10. Obviously, the carbonation reaction has the largest reaction rate on the (0 0 1) − 1 surface of K_2CO_3 with a hexagonal structure, which is 9.39×10^7 s^{-1}, far more than that on a K_2CO_3/TiO_2 surface. These results indicate that bicarbonate formation is not feasible at the interface of K_2CO_3/TiO_2 through the reaction with "one-step mechanism".

For the "two-step mechanism" (i.e., H_2O dissociates preceding bicarbonate formation, then proton H transfers to CO_3 anions, and OH group from the H_2O dissociation reacts with the gas molecule of CO_2), all reactions used for calculation are summarized in Table 5 (R2–R5). As OH was found in the carbonation reaction, we therefore first considered H_2O adsorption and dissociation. Reaction (2) (R2) was supposed to be equilibrium. The other step, R3, was described by the forward rate. The site balance of intermediate species included in the reaction mechanism can be written in terms of coverage (θ_X; X = surface species) for reactions (2) and (3).

$$\theta_{H_2O} + \theta_H + \theta_{HO} + \theta^* = 1 \quad (15)$$

The θ^* is the coverage of vacancy. The coverage of H_2O is calculated as follows:

$$\theta_{H_2O} = P_{H_2O}K_{H_2O}\theta^* \quad (16)$$

The θ_H and θ_{HO} can be calculated according to the formula below:

$$\theta_H = \theta_{HO} = k_3\theta_{H_2O}\theta^* \quad (17)$$

By putting Eqs. (16) and (17) into (15), we can calculate θ^* and surface coverage of other species according to the equilibrium-state approximation presented as follows:

$$P_{H_2O}K_{H_2O}\theta^* + 2k_3P_{H_2O}K_{H_2O}\theta^*\theta^* + \theta^* = 1 \quad (18)$$

According to these equations, we can obtain the result of θ_{HO}. So the carbonation reaction (R5) rate on per site could be calculated by the

Table 4
Transition state structure parameters, activation energies E_a and reaction energies ΔE for co-adsorption CO_2 and H_2O reaction on K_2CO_3/TiO_2(1 1 0).

Configuration	r(C–O) (Å)	r(C–O) (Å)	r(H1–O_w)[a] (Å)	r(H2–O_w)[a] (Å)	r(C–O) (Å)	O-C-O (°)	E_a (kJ·mol^{-1})	ΔE (kJ·mol^{-1})
TS1	1.202	1.221	0.981	2.481	2.108	152.3	146.6	66.6

[a] The O_w is refer to O atom of H_2O molecule.

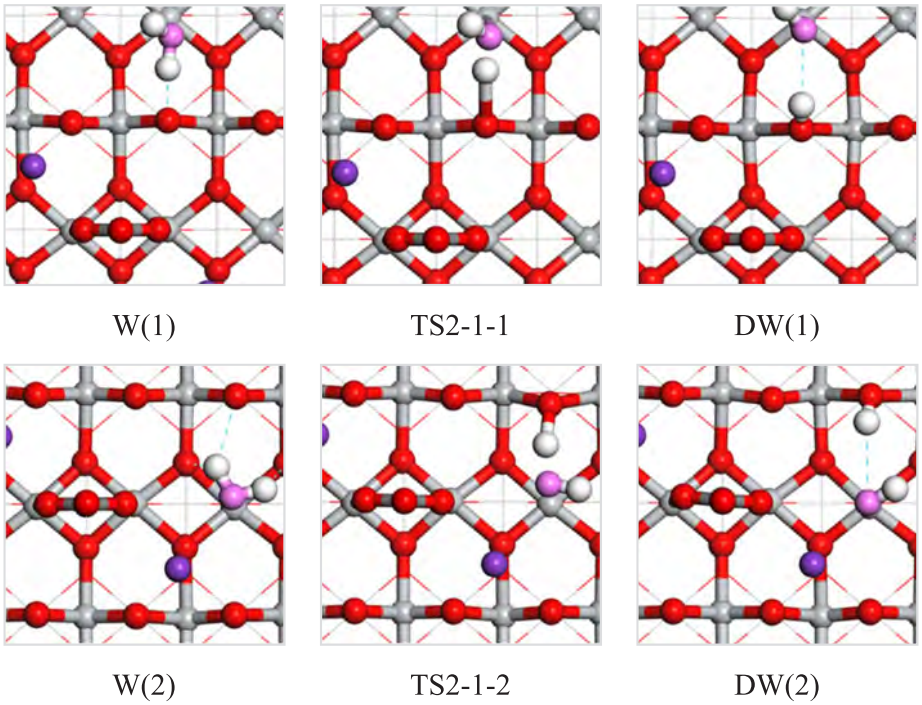

Fig. 7. The dissociation of a H_2O molecule over the K_2CO_3 loaded on TiO_2 (1 1 0) surfaces.

Table 5
Transition state structure parameters, activation energies E_a and reaction energies ΔE for H_2O dissociative on K_2CO_3/TiO_2 (1 1 0).

Configurations	r(Ti-O_w)[a] (Å)	r(O_b-H)[b] (Å)	r(K-O_w)[a] (Å)	r(O_w-H)[a] (Å)	E_a (kJ·mol^{-1})	ΔE (kJ·mol^{-1})
TS2-1-1	2.240	1.417	–	1.485	48.2	8.7
TS2-1-2	2.169	1.468	3.014	1.171	37.6	-13.5

[a] The O_w is refer to O atom of HO molecule.
[b] The O_b is refer to a generic surface bridging O atom.

Table 6
Transition state structure parameters, activation energies E_a and reaction energies ΔE for reaction of H proton transfer reaction from OH_b group to the O atoms of CO_3 anions.

Configurations	r(O_c-H)[a] (Å)	r(O_b-H)[b] (Å)	E_a (kJ·mol^{-1})	ΔE (kJ·mol^{-1})
TS2-2-1	1.389	1.480	54.0	19.3
TS2-2-2	1.635	2.005	59.8	-8.7

[a] The O_w is refer to O atom of CO_3 species.
[b] The O_b is refer to a generic surface bridging O atom.

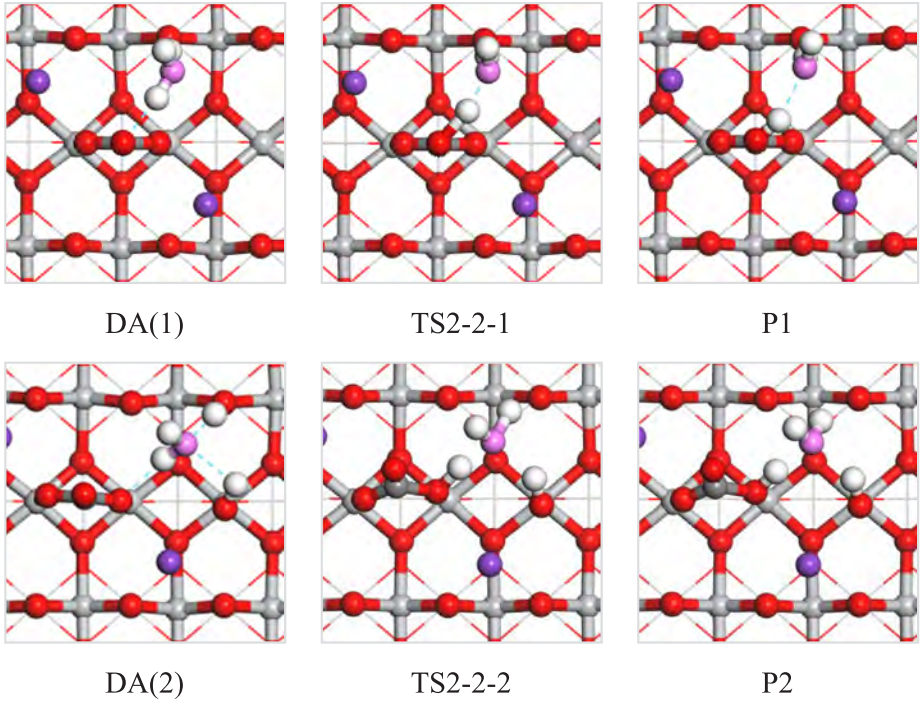

Fig. 8. The pathways for reaction of H proton transfer reaction from OH_b group to the O atoms of CO_3 anions. For increased clarity, the oxygen atoms of H_2O are indicated in pink, and the oxygen atoms of the slab are indicated in red. (For interpretation of the references to color in this figure legend, the reader is referred to the web version of this article.)

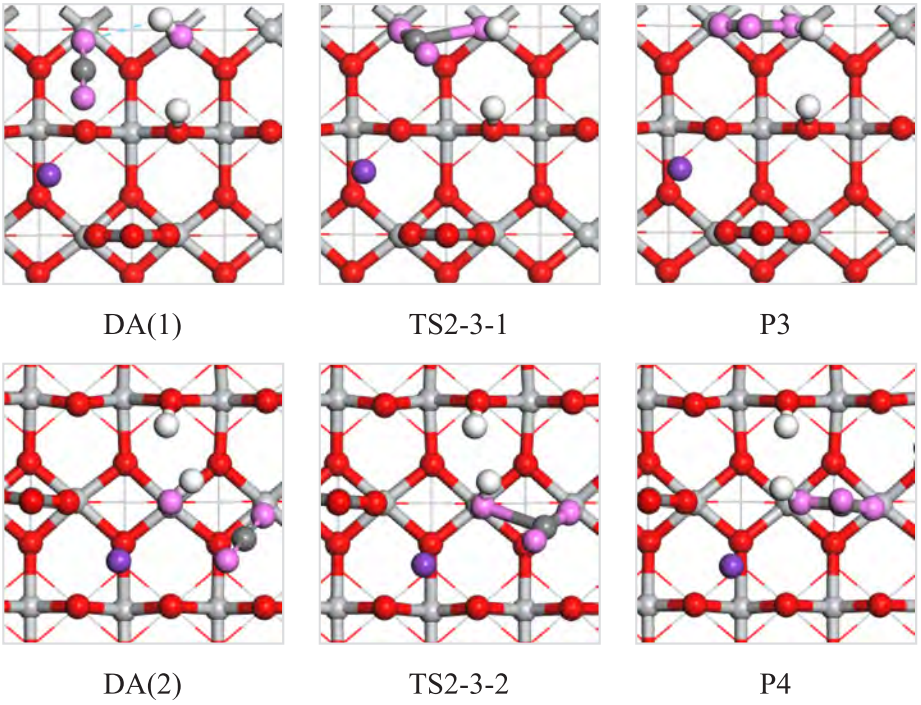

Fig. 9. The pathways for reaction of the OH_t attacking a nearby CO_2 molecule adsorbed on K_2CO_3/TiO_2. For increased clarity, the oxygen atoms of OH_t and H_2O are indicated in pink, and the oxygen atoms of the slab are indicated in red. (For interpretation of the references to color in this figure legend, the reader is referred to the web version of this article.)

Table 7
Transition state structure parameters, activation energies E_a and reaction energies ΔE for gas CO_2 and OH_t reaction on K_2CO_3/TiO_2(1 1 0).

Surfaces	r(C–O1) (Å)	r(C–O2) (Å)	r(H1–O) (Å)	r(C–O_w)[a] (Å)	O-C-O[d] (°)	E_a (kJ·mol^{-1})	ΔE (kJ·mol^{-1})
TS2-3-1	1.204	1.226	0.967	1.958	141.5	44.4	−7.7
TS2-3-2	1.196	1.215	0.973	2.261	155.2	57.9	−28.9

[a] The O_w is refer to O atom of OH_t molecule.

Table 8
The relevant elementary reactions of bicarbonate formation on the surface of TiO_2 (1 1 0) and at the interface of K_2CO_3/TiO_2 (1 1 0) together with the corresponding activation free energies G_a (kJ·mol^{-1}), reaction free energies ΔG (kJ·mol^{-1}) and rate constant k (s^{-1}) at 350 K.

Elementary reactions		On the surface			At the interface		
		G_a	ΔG	k	G_a	ΔG	k
R1	$CO_2(g) + * \leftrightarrow CO_2^*$	–	–	–	–	–	–
R2	$H_2O(g) + * \leftrightarrow H_2O^*$	–	–	–	–	–	–
R3	$H_2O^* + * \overset{k_3}{\rightarrow} HO^* + H^*$	46.4	6.8	6.33×10^5	18.3	−14.7	6.89×10^9
R4	$H^* + CO_3^* \overset{k_4}{\rightarrow} HCO_3^*$	53.3	17.5	1.04×10^5	62.8	−10.5	1.12×10^3
R5	$HO^* + CO_2(g) \overset{k_5}{\rightarrow} HCO_3^*$	27.7	−7.4	4.92×10^8	37.4	−24.5	3.54×10^7
R6	$CO_2^* + H_2O^* \overset{k_6}{\rightarrow} HCO_3^* + H^*$	–	–	–	148.8	68.8	2.06×10^{-10}

Table 9
The Gibbs adsorption free energy (kJ·mol^{-1}) and equilibrium constant of CO_2 and H_2O adsorption on the K_2CO_3/TiO_2 sorbent at 350 K.

Adsorbates	Free energy of adsorption	Equilibrium constant
C(1)	−31.7	3.78×10^5
C(2)	−30.4	2.88×10^5
W(1)	−70.6	6.15×10^{10}
W(2)	−80.5	3.49×10^{12}

following formula:

$$r_5 = k_5 \theta_{HO} P_{CO_2} \quad (19)$$

The calculated θ_{H_2O}, θ_H and θ_{HO} are 9.96×10^{-1}, 6.81×10^{-5} and 6.82×10^{-5} on the surface of TiO_2 (1 1 0), respectively, while they are 9.74×10^{-1}, 1.25×10^{-2} and 1.25×10^{-2} at the interface of K_2CO_3/TiO_2(1 1 0). Next, the reaction rate for H_2O dissociation and bicarbonate formation (H transfer and OH group reacting with the gas molecule of CO_2) are calculated by $r_3 = k_3 \theta_{H_2O} \theta^*$, $r_4 = k_4 \theta_H$ and $r_5 = k_5 \theta_{OH} P_{CO_2}$; the corresponding values are 6.81×10^{-5}, 7.08 and 5.03×10^3 s^{-1} on the surface of TiO_2 (1 1 0), and 1.25×10^{-2}, 1.40×10^1 and 6.64×10^4 s^{-1} at the interface of K_2CO_3/TiO_2 (1 1 0), respectively.

Obviously, the bicarbonate formation reaction rates of R6 are much lower than those of R4 and R5; therefore, it is impossible for bicarbonate formation through the "one-step mechanism". In our previous work [14] on pure K_2CO_3, the carbonation reaction occurs through both the "one-step mechanism" and "two-step mechanism". Certainly, the mechanism is different from that on pure K_2CO_3 when TiO_2 support exists. It is noted that the step of H transfer appears in the "two-step

Table 10
The equilibrium constant and coverage of CO_2 and H_2O adsorption, rate constant k and reaction rate$r$ for CO_2 and H_2O reaction on the monoclinic and hexagonal K_2CO_3 each surfaces through "one-step mechanism", respectively (T = 350 K).

Surfaces		k_6 (s^{-1})	K_{CO_2}	K_{H_2O}	θ_{CO_2}	θ_{H_2O}	r_6 (s^{-1})
Monoclinic	(0 0 1)	2.65×10^{9}	3.53×10^{6}	2.39×10^{15}	1.48×10^{-9}	1.00×10^{0}	3.92×10^{0}
	(0 1 1)	3.15×10^{5}	1.28×10^{6}	9.69×10^{10}	1.32×10^{-5}	1.00×10^{0}	4.15×10^{0}
	(1 0 0)	4.81×10^{10}	4.55×10^{7}	2.49×10^{13}	1.83×10^{-6}	1.00×10^{0}	8.79×10^{4}
	(1 1 1)	2.89×10^{7}	1.59×10^{12}	7.98×10^{15}	1.99×10^{-4}	1.00×10^{0}	5.76×10^{3}
	(1 0 1)	2.83×10^{6}	1.12×10^{7}	1.19×10^{16}	9.43×10^{-10}	1.00×10^{0}	2.67×10^{-3}
	(1 1 0)	1.54×10^{9}	1.89×10^{5}	3.71×10^{10}	5.11×10^{-6}	1.00×10^{0}	7.85×10^{3}
	(0 1 0)	3.86×10^{8}	5.91×10^{7}	4.92×10^{16}	1.20×10^{-9}	1.00×10^{0}	4.64×10^{-1}
Hexagonal	(1 1 1)	1.52×10^{8}	4.05×10^{5}	1.06×10^{14}	3.83×10^{-9}	1.00×10^{0}	5.81×10^{-1}
	(0 1 1)	3.58×10^{9}	4.41×10^{6}	1.20×10^{12}	3.67×10^{-6}	9.99×10^{-1}	1.31×10^{4}
	(1 1 0)	7.82×10^{9}	5.76×10^{3}	3.51×10^{11}	1.64×10^{-8}	1.00×10^{0}	1.28×10^{2}
	(0 0 1)−1	5.41×10^{8}	9.67×10^{10}	3.36×10^{11}	2.23×10^{-1}	7.77×10^{-1}	9.39×10^{7}
	(0 0 1)−2	4.02×10^{8}	5.09×10^{3}	1.46×10^{10}	3.48×10^{-7}	1.00×10^{0}	1.40×10^{2}
	(0 1 0)	3.67×10^{8}	2.21×10^{7}	2.18×10^{11}	1.01×10^{-4}	1.00×10^{0}	3.72×10^{4}

Table 11
The equilibrium constant and coverage of H_2O adsorption, coverage of OH group, rate constant and reaction rate for H_2O dissociation r_3 as well as CO_2 and HO reaction r_5 on the monoclinic and hexagonal K_2CO_3 each surfaces through "two-step mechanism", respectively (T = 350 K).

Surfaces		k_3 (s^{-1})	k_5 (s^{-1})	K_{H_2O}	θ_{H_2O}	θ_{HO}	r_3 (s^{-1})	r_5 (s^{-1})
Monoclinic	(0 0 1)	2.17×10^{-10}	8.89×10^{11}	2.39×10^{15}	1.00	6.06×10^{-25}	6.06×10^{-25}	8.08×10^{-14}
	(0 1 1)	5.56×10^{-6}	2.25×10^{13}	9.69×10^{10}	1.00	3.83×10^{-16}	3.83×10^{-16}	1.29×10^{-3}
Hexagonal	(0 1 0)	2.38×10^{4}	2.31×10^{10}	2.18×10^{11}	1.00	7.28×10^{-7}	7.28×10^{-7}	2.52×10^{3}

mechanism" over TiO_2 supported K_2CO_3 sorbent compared to that on pure K_2CO_3 sorbent, where H dissociated from H_2O, need not transfer but directly bonds to CO_3 to form HCO_3. On the other hand, the reaction rates of R3, R4 and R5 are comparable to each other at the interface of K_2CO_3/TiO_2 or on the surface of TiO_2, and the rate-determining steps are likely governed by reaction step R3, i.e., the H_2O dissociation process is the rate-determining step of the carbonation reaction. Mahinpey et al. [28] proposed an initial rate-determining step is H_2O adsorption step, and the reaction mechanism follows below equations:

$$K_2CO_3\ (s) + H_2\ O\ (g) \Leftrightarrow K_2\ CO_3{\cdot}[H_2\ O]_{ads} \quad (20)$$

$$K_2CO_3\ [H_2O]_{ads} + CO_2\ (g) \Leftrightarrow 2KHCO_3\ (s) \quad (21)$$

However, the detailed reaction is still not clarified about $K_2CO_3{\cdot}[H_2O]_{ads}$ reacting with CO_2. Herein, we proposed that the mechanism is (1) chemisorbed H_2O is dissociated into OH and H, then (2) OH is combined with physisorbed CO_2 into HCO_3 on the K_2CO_3/TiO_2 sorbent, and at the time, H is transferred through the surface and combined with CO_3 from K_2CO_3 into HCO_3. Furthermore, the values of reaction rates at the interface are about 3 orders of magnitude higher than the corresponding values on the surface, which indicates that the interface of K_2CO_3/TiO_2 offers better active sites for CO_2 capture. When K_2CO_3 is supported on TiO_2 (1 1 0), the carbonation reaction is accelerated compared to that on a pure K_2CO_3 surface under real reaction conditions (the reaction rate on pure K_2CO_3 is listed in Table 11). Obviously, the addition of a TiO_2 support promotes the dissociation of the H_2O molecule, which makes the carbonation reaction accelerate, compared to the pure K_2CO_3 surface.

Although the addition of a TiO_2 support promotes the dissociation of H_2O, the overall reaction rate is still not increased. Because H_2O dissociation is the rate-determining step, according to our kinetic modeling, accelerating the dissociation of H_2O will further increase the coverage of OH, thus strengthening the capture ability of K_2CO_3/TiO_2 to CO_2. The suggestion may be confirmed by the following experiments. For example, $TiO(OH)_2$ has been reported as a great catalytic support for CO_2 capture leading to a significant increase of CO_2 sorption capacity per unit of K_2CO_3 by a factor of about 37 [24]. Furthermore, this group confirmed that $TiO(OH)_2$/tetraethylenepentamine is a good sorbent for CO_2 capture [25]. In the real application, it is proposed that adding promote to the K_2CO_3/TiO_2 sorbent which can improve the dissociation rate of H_2O, or pretreating the K_2CO_3/TiO_2 sorbent to create more OH on the surface of the sorbent so that it is accelerated for CO_2 capture.

4. Conclusions

The capture of CO_2 using K_2CO_3 loaded on rutile of TiO_2 has been studied using corrected DFT slab calculations. The active sites of CO_2 and H_2O adsorption as well as the detail mechanism of CO_2 capture by K_2CO_3/TiO_2 (1 1 0), are present. The results show that, over the K_2CO_3 supported on a (4 × 2) TiO_2 (1 1 0) surface, CO_2 and H_2O prefer to adsorb at the interface between the TiO_2 and K_2CO_3. Meanwhile, their adsorptions are weaker than those on pure K_2CO_3. The H_2O, as well as co-adsorbed OH and H species, bind much more strongly than does the CO_2 molecule. Further, co-adsorbed H_2O, as well as OH and H species, can slightly increase the adsorption ability of the CO_2 molecule on the sorbent, which is similar to the previous research on CO_2 and H_2O adsorbed on pure K_2CO_3 surfaces and pure TiO_2 surfaces. The carbonation reaction is processed not via a "one-step mechanism" but via a "two-step mechanism", i.e., the adsorbed H_2O molecule dissociates to form OH_t adsorbed at the top Ti site and H_b species adsorbed at the bridging of the O site. The CO_3 anion then deprives the transferred H_b group, at the same time, the gas CO_2 molecule reacts with the OH_t group, leading to the production of the bicarbonate group. More importantly, the reaction prefers to occur at the interface of K_2CO_3/TiO_2, and H transfer step is added when K_2CO_3 is loaded on the support TiO_2 compared that on pure K_2CO_3.

The kinetic modeling results show that the carbonation reaction is governed by H_2O dissociation. The dissociation of H_2O may limit the carbonation reaction. Therefore, either H_2O-dissociative or high OH coverage support material should be the most promising candidates for maximizing the carbonation performance of a K_2CO_3-based solid sorbent in practice.

Acknowledgments

This work was supported financially by Key Projects of National Natural Science Foundation of China (21736007), the National Natural Science Foundation of China (Nos. 21506120 and 21576178).

References

[1] Allen MR, Frame DJ, Huntingford C, Jones CD, Lowe JA, Meinshausen M, et al. Warming caused by cumulative carbon emissions towards the trillionth tonne. Nature 2009;458:1163–6.
[2] Aaron D, Tsouris C. Separation of CO_2 from flue gas: a review. Sep Sci Technol 2005;40:321–48.
[3] Wilson M, Tontiwachwuthikul P, Chakma A, Idem R, Veawab A, Aroomwilas A, et al. Test results from a CO_2 extraction pilot plant at boundary dam coal-fired power station. Energy 2004;29:1259–67.
[4] Freund P, Ormerod WG. Progress toward storage of carbon dioxide. Energy Convers Manage 1997;38:S199–204.
[5] Mavroudi M, Kaldis SP, Sakellaropoulos GP. Reduction of CO_2 emissions by a membrane contacting process. Fuel 2003;82:2153–9.
[6] Zhang X, Zhang X, Liu H, Li W, Xiao M, Gao H, et al. Reduction of energy requirement of CO_2 desorption from a rich CO_2-loaded MEA solution by using solid acid catalysts. Appl Energ 2017;202:673–84.
[7] Cheng C, Li K, Yu H, Jiang K, Chen J, Feron P. Amine-based post-combustion CO_2 capture mediated by metal ions: advancement of CO_2 desorption using copper ions. Appl Energ 2018;211:1030–8.
[8] Chen SJ, Zhu M, Fu Y, Huang YX, Tao ZC, Li WL. Using 13X, LiX, and LiPdAgX zeolites for CO_2 capture from post-combustion flue gas. Appl Energ 2017;191:87–98.
[9] Khelifa A, Benchehida L, Derriche Z. Adsorption of carbon dioxide by X zeolites exchanged with Ni^{2+} and Cr^{3+}: isotherms and isosteric heat. J Colloid Interface Sci 2004;278:9–17.
[10] Yi CK, Jo SH, Seo Y, Park SD, Moon KH, Yoo JS, et al. CO_2 capture characteristics of dry sorbents in a fast fluidized reactor. Stud Surf Sci Catal 2006;159:501–4.
[11] Lee SC, Choi BY, Lee SJ, Jung SY, Chong KR. CO_2 absorption and regeneration using Na and K based sorbents. Stud Surf Sci Catal 2004;153:527–30.
[12] Lee JM, Min YJ, Lee KB, Jeon SG, Na JG, Ryu HJ. Enhancement of CO_2 sorption uptake on hydrotalcite by impregnation with K_2CO_3. Lagmuir 2010;26:18788–97.
[13] Hanif A, Dasgupta S, Divekar S, Arya A, Garg MO, Nanoti A. A study on high temperature CO_2 capture by improved hydrotalcite sorbents. Chem Eng J 2014;15:91–9.
[14] Liu H, Qin Q, Zhang R, Ling L, Wang B. Insight into the mechanism of the capture of CO_2 by K_2CO_3 sorbent: a DFT study. Phys Chem Chem Phys 2017;19:24357–68.
[15] Lee SC, Choi BY, Lee TJ, Kim JC. CO_2 absorption and regeneration of alkali metal-based solid sorbents. Catal Today 2006;111:385–90.
[16] Lee SC, Kim JC. Dry potassium-based sorbents for CO_2 capture. Catal Surv Asia 2007;11:171–85.
[17] Lee SC, Chae HJ, Lee SJ, Kim JC. Novel regenerable potassium-based dry sorbents for CO_2 capture at low temperatures. J Mol Catal B-Enzym 2009;56:179–84.
[18] Lee SC, Chae HJ, Kwon YM, Kim JC. Characteristics of new potassium-based sorbents prepared with nano-titanium oxide for carbon dioxide capture. J Nanoelectron Optoe 2010;5:212–7.
[19] Guo Y, Zhao C, Li C, Lu S. Application of PEI-K_2CO_3/AC for capturing CO_2 from flue gas after combustion. Appl Energ 2014;129:17–24.
[20] Zhao C, Chen X, Zhao C. Carbonation behavior of K_2CO_3 with different microstructure used as an active component of dry sorbents for CO_2 capture. Ind Eng Chem Res 2010;49:12212–6.
[21] Li L, Li Y, Wen X, Sun Y. CO_2 capture over K_2CO_3/MgO/Al_2O_3 dry sorbent in a fluidized bed. Energy Fuel 2011;25:3835–42.
[22] Zhao C, Chen X, Zhao C. K_2CO_3/Al_2O_3 for capturing CO_2 in flue gas from power plants. Part 1: carbonation behaviors of K_2CO_3/Al_2O_3. Energy Fuel 2012;26:1401–5.
[23] Lee SC, Kwon YM, Park YH, Lee WS, Park JJ, Ryu CK, et al. Structure effects of potassium-based TiO_2 sorbents on the CO_2 capture capacity. Top Catal 2010;53:641–7.
[24] Tuwati A, Fan M, Russell AG, Wang J, Dacosta HFM. New CO_2 sorbent synthesized with nanoporous $TiO(OH)_2$ and K_2CO_3. Energy Fuel 2013;27:7628–36.
[25] Irani M, Gasem K, Ditcher B, Fan M. CO_2 capture using nanoporous $TiO(OH)_2$ /tetraethylenepentamine. Fuel 2016;183:601–8.
[26] Lai Q, Toan1 S, Assiri MA, Cheng H, Russell AG, Adidharma H, Radosz M, Fan M. Catalyst-$TiO(OH)_2$ could drastically reduce the energy consumption of CO_2 capture. Nat Commun 2018;9:2672.
[27] Jayakumar A, Gomez A, Mahinpey N. Post-combustion CO_2 capture using solid K_2CO_3: discovering the carbonation reaction mechanism. Appl Energ 2016;179:531–43.
[28] Jayakumar A, Gomez A, Mahinpey N. Kinetic behavior of solid K_2CO_3 under postcombustion CO_2 capture conditions. Ind Eng Chem Res 2017;56:853–63.
[29] Zhao CW, Chen XP, Zhao CS. Carbonation and active-component-distribution behaviors of several potassium-based sorbents. Ind Eng Chem Res 2011;50:4464–70.
[30] Lee S, Chae H, Choi B, Jung S, Ryu C, Park J, et al. The effect of relative humidity on CO_2 capture capacity of potassium-based sorbents. Korean J Chem Eng 2010;28:480–6.
[31] Zhao W, Sprachmann G, Li Z, Cai N. Zhang X. Effect of K_2CO_3·1.5H_2O on the regeneration energy consumption of potassium-based sorbents for CO_2 capture. Appl Energ 2013;112:381–7.
[32] Gao H, Pishney S, Janik MJ. First principles study on the adsorption of CO_2 and H_2O on the K_2CO_3 (001) surface. Sur Sci 2013;609:140–6.
[33] Zhao W, Wu Y, Cai T, Zhang W, Chen X, Liu D. Density functional theory and reactive dynamics study of catalytic performance of TiO_2 on CO_2 desorption process with $KHCO_3$/TiO_2/Al_2O_3 sorbent. Mol Catal 2017;439:143–54.
[34] Sorescu DC, Lee J, Al-Saidi WA, Jordan KD. Coadsorption properties of CO_2 and H_2O on TiO_2 rutile (110): a dispersion-corrected DFT study. J Chem Phys 2012;137:074704.
[35] Yin W, Krack M, Wen B, Ma S, Liu L. CO_2 capture and conversion on rutile TiO_2(110) in the water environment: insight by first-principles calculations. J Phys Chem Lett 2015;6:2538–45.
[36] Yin W, Wen B, Bandaru S, Krack M, Lau M, Liu L. The effect of excess electron and hole on CO_2 adsorption and activation on rutile (110) surface. Sci Rep 2016;6:23298.
[37] Clark SJ, Segall MD, Pickard CJ, Hasnip PJ, Probert MIJ, Refson K, et al. First principles methods using CASTEP. Z Kristallogr 2005;220:567–70.
[38] Segall MD, Lindan PJD, Probert MJ, Pickard CJ, Hasnip PJ, Clark SJ, et al. First-principles simulation: ideas, illustrations and the CASTEP code. Phys: Condens Mat 2002;14:2717–44.
[39] Karlsen EJ, Nygren MA, Pettersson LGM. Comparative study on structures and energetics of NO_x, SO_x, and CO_x adsorption on alkaline-earth-metal oxides. J Phys Chem B 2003;107:7795–802.
[40] Schneider WF. Qualitative differences in the adsorption chemistry of acidic (CO_2, SO_x) and amphiphilic (NO_x) species on the alkaline earth oxides. J Phys Chem B 2004;108:273–82.
[41] Hong QJ, Liu ZP. Mechanism of CO_2 hydrogenation over Cu/ZrO_2 (212) interface from first-principles kinetics monte carlo simulations. Surf Sci 2010;604:1869–76.
[42] Wu D, Jiang W, Liu X, Xue Y. Theoretical study about effects of H_2O and Na^+ on adsorption of CO_2 on kaolinite surfaces. Chem Res Chin U 2016;32:118–26.
[43] Kurth S, Perdew JP, Blaha P. Molecular and solid-state tests of density functional approximations: LSD, GGAs, and meta-GGAs. Int J Quant Chem 1999;75:889–909.
[44] Grimme S, Ehrlich S, Goerigk L. Effect of the damping function in dispersion corrected density functional theory. J Comput Chem 2011;32:1456–65.
[45] Monkhorst HJ, Pack JD. Special points for brillouin-zone integrations. Phys Rev B 1976;13:5188–92.
[46] Cao XM, Burch R, Hardacre C, Hu P. An understanding of chemoselective hydrogenation on crotonaldehyde over Pt (111) in the free energy landscape: the microkinetics study based on first-principles calculations. Catal Today 2011;165:71–9.
[47] Choi YM, Liu P. Mechanism of ethanol synthesis from syngas on Rh (111). J Am Chem Soc 2009;131:13054–61.
[48] Ramamoorthy M, King-Smith RD, Vanderbilt D. First-principles calculations of the energetics of stoichiometric TiO_2 surfaces. Phys Rev B 1994;49:7709.
[49] Henrich VE, Cox PA, Diebold U. The surface science of metal oxides: the surface science of metal oxides. Cambridge University Press; 1994. 138–138.
[50] Baltrusaitis J, Jensen JH, Grassian VH. FTIR spectroscopy combined with isotope labeling and quantum chemical calculations to investigate adsorbed bicarbonate formation following reaction of carbon dioxide with surface hydroxyl groups on Fe_2O_3 and Al_2O_3. J Phys Chem B 2006;110:12005–16.
[51] Grinter DC, Remesal ER, Luo S, Evans J, Senanayake SD, Stacchiola DJ, et al. Potassium and water coadsorption on TiO2 (110): OH-induced anchoring of potassium and the generation of single-site catalysts. J Phys Chem Lett 2016;7:3866–72.
[52] Samanta A, Zhao A, Shimizu GKH, Sarkar P, Gupta R. Post-combustion CO_2 capture using solid sorbents: a review. Ind Eng Chem Res 2012;51:1438–63.
[53] Bandura AV, Sykes DG, Shapovalov V, Troung TN, Kubicki JD, Evarestov RA. Adsorption of water on the TiO_2 (rutile) (110) surface: a comparison of periodic and embedded cluster calculations. J Phys Chem B 2004;108:7844–53.
[54] Sahoo SK, Nigam S, Sarkar P, Majumder C. DFT study of H_2O adsorption on TiO_2 (110) and SnO_2 (110) surfaces. AIP Conf Proc 2013;1512:292–3.
[55] Perron H, Vandenborre J, Domain C, Drot R, Roques J, Simoni E, et al. Combined investigation of water sorption on TiO_2 rutile (110) single crystal face: XPS vs. periodic DFT. Surf Sci 2007;601:518–27.
[56] Sebbari K, Domain C, Roques J, Perron H, Simoni E, Catalette H. Investigation of hydrogen bonds and temperature effects on the water monolayer adsorption on rutile TiO_2 (110) by first-principles molecular dynamics simulations. Surf Sci 2011;605:1275–80.
[57] Henderson MA. Evidence for bicarbonate formation on vacuum annealed TiO_2 (110) resulting from a precursor-mediated interaction between CO_2 and H_2O. Surf Sci 1998;400:203–19.